

High-Dispersion Spectroscopy of AE Aqr – II: evidence of material orbiting the primary star

S. H. Ramírez^{1*} and J. Echevarría¹

¹ Instituto de Astronomía, Universidad Nacional Autónoma de México, Apartado Postal 70-264, Ciudad Universitaria, México D.F., C.P. 04510,

Accepted XXX. Received YYY; in original form ZZZ

ABSTRACT

We present a second paper of the analyses of high-dispersion spectroscopic observations of the magnetic cataclysmic variable AE Aquarii. We focus our efforts on the study of the emission lines and their radial velocities. We detect a sinusoidal behaviour, in several of the observing runs, with variable amplitudes. Of those runs presented, the velocity curve of 2000 August shows less instability in the emission material. In this case we obtain $K_1 = 114 \pm 8 \text{ km s}^{-1}$, which we take as our best value for the radial velocity of the primary. This result is consistent within 2σ with previously published values obtained using indirect methods. We interpret this consistency as observational evidence of material orbiting the rapidly-rotating primary star. We present a Doppler Tomography study, which shows that the $H\alpha$ emission is primarily concentrated within a blob in the lower left quadrant; a structure similar to that predicted by the propeller model. However, for 2000 August, we find the emission centred around the position of the white dwarf, which supports the possibility of the K_1 value of this run of being a valid approximation of the orbital motion of the white dwarf.

Key words: Cataclysmic Variables – Spectroscopic – Radial Velocities, star:individual-

1 INTRODUCTION

Cataclysmic variables (CVs) are interacting binaries, that consist of a white dwarf (WD) primary star and a late-type main sequence star (secondary), that transfers matter to the primary via Roche Lobe overflow (see Warner 1995, and references therein).

In the classical model, established by Smak (1971) and Warner & Nather (1971), the material transferred from the secondary flows through the inner Lagrangian point and orbits around the primary forming an accretion disc. However, if the magnetic field of the WD is very strong ($\geq 10 \text{ MG}$), it inhibits the formation of a disc and the material is channeled by the field lines towards the magnetic poles of the WD, as is the case in the so called polar systems (see Kafka et al. 2005, and references therein). Furthermore the magnetic field lines can lock the rotation of the compact star with the orbital period (see Cropper 1990). Alternately, if the magnetic field is not strong enough (0.1-10 MG), a partial external disc determined by the Alfvén radius is formed, where the internal part of the disc is threaded by the field, and caused to flow along the field lines. In this case the strength of the field is not sufficient to synchronise the rotation of the WD with the orbital period. These systems are known as intermediate polars (see Patterson 1994, and references therein).

Given that CVs are spectroscopic binaries, the study of the radial velocities of their components is paramount to obtain the orbital parameters. Moreover, by means of a method

called Doppler Tomography, developed by Marsh & Horne (1988), the Doppler shifts of the emission lines are analysed as a function of the orbital phase, to create a two-dimensional map of the binary system in velocity space.

AE Aqr is a nova-like CV whose components are a rapidly rotating magnetic WD, with a 33 s spin period (Patterson 1979); and a late-type companion with a spectral type of K0-K4 (Echevarría et al. 2008, hereinafter Paper I). The binary has an unusually long orbital period of 9.88 h (Walker 1965).

The system was first characterised as an intermediate polar by Patterson (1979). The moderate intensity of the WD’s magnetic field (Cropper 1986) should permit the partial formation of a disc. However, spectroscopic observations do not show a double-peaked structure in the Balmer emission lines (e.g. Robinson et al. 1991; Welsh et al. 1998); a structure characteristic in the line profiles of discs in systems of high inclination (see Horne & Marsh 1986). Furthermore, no signature of a disc was found in the Doppler tomograms put forward by Wynn et al. (1997) and Welsh et al. (1998). These authors, with proper caution, interpreted this as possible evidence that the material transferred from the secondary was being ejected by the rapidly-rotating magnetic field of the WD, which acted as a propeller at the time of their observations. Indeed, numerical magnetohydrodynamics simulations (Isakova et al. 2016; Blinova et al. 2019) predict that, when in a propeller regime, an oscillating and rather unstable disc of a transient nature, is able to form around the WD of AE Aqr, which would be difficult to detect in Doppler tomograms. So as was succinctly put by Wynn et al. (1997): *AE Aqr is likely to alternate between phases of disc accretion, in which the*

* e-mail: sergio.ramirez@ciencias.unam.mx

white dwarf spins up, and propeller states in which it spins down.

In this article, we use the same UCLES and Echelle observations published in Paper I, who deferred the analysis of the emission lines for a later study. In particular, we use the observations of 1991 Aug and 2000 Aug (See Section 2 of Paper I). We also analyse an unpublished third set of observations from 2008 Aug. We will briefly describe all three observing runs in Section 2. We present a radial velocity analysis in Section 3, followed by a Doppler Tomography study in Section 4. We close this paper with a discussion of the results in Section 5 and our conclusions in Section 6.

2 OBSERVATIONS

Spectroscopic observations of AE Aqr were made using the Anglo-Australian Telescope (AAT) and the University College London Echelle Spectrograph (UCLES) at the coude focus, on 1991, August 2 and 3. A total of 102 spectra of 360 s exposure each, were obtained, with a typical signal to noise ratio of 10 (around $\lambda 4500 \text{ \AA}$). We used a $31.6 \text{ lines mm}^{-1}$ grating and a Blue Thomson 1024 x 1024 CCD with the 700 mm camera. The spectral region of $\lambda 4000 \text{ \AA}$ to $\lambda 5100 \text{ \AA}$ was covered, with a spectral resolution of about 5.4 kms^{-1} . Almost two complete orbital periods were covered. Several late-type standard stars were also observed.

Two further runs were carried out at the Observatorio Astronómico Nacional at San Pedro Mártir (SPM) using the 2.1m Telescope and the Echelle Spectrograph.

In the second set of observations, made during the nights of 2000 August 17 and 19, 81 spectra of 600 s exposure were obtained, using a 15μ Thomson 2048 x 2048 detector and a 300 lines mm^{-1} echellette grating to cover a spectral range from $\lambda 3700 \text{ \AA}$ to $\lambda 7700 \text{ \AA}$, with a typical signal to noise ratio of 42 (around $\lambda 5450 \text{ \AA}$).

The third run of observations were made during the nights of 2008 August 14 and 16-20. A total of 171 spectra of 600 s exposure were obtained. A $15\mu\text{m}$ SITe3 1024 x 1024 detector was employed, covering a spectral interval from $\lambda 3970$ to $\lambda 6650 \text{ \AA}$, with a typical signal to noise ratio of 30 (around $\lambda 5450 \text{ \AA}$).

3 RADIAL VELOCITY ANALYSIS OF THE PRIMARY STAR

We measured the radial movement of the wings of the $H\alpha$ and $H\beta$ lines, using two Gaussian functions with a fixed width and separation as described by Shafter et al. (1986). We fit the radial velocities measured from the full set of spectra to a circular orbit:

$$V(t) = \gamma + K \sin\left(2\pi \frac{t - t_0}{P_{orb}}\right), \quad (1)$$

where γ is the systemic velocity, K the semi-amplitude, t_0 the time of inferior conjunction of the donor, and P_{orb} is the orbital period. We employed χ^2 as our goodness-of-fit parameter. Following the methodology carried out by Horne et al. (1986), the orbital period was fixed in Equation 1, and therefore only the other three parameters were calculated. Since the orbital period has been well established in Paper I, we use the published value of 0.4116554800(2) days.

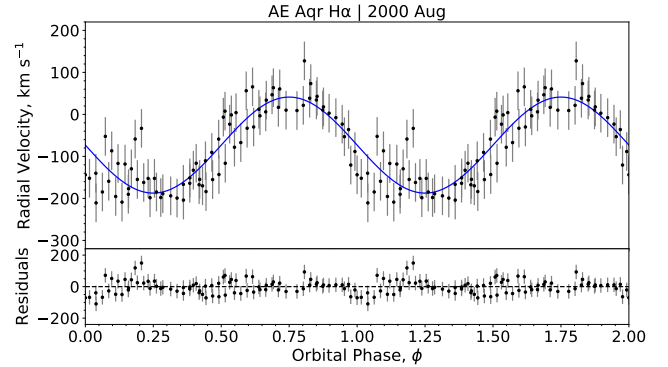


Figure 1. Radial velocity curve of $H\alpha$ for the 2000 Aug observation run.

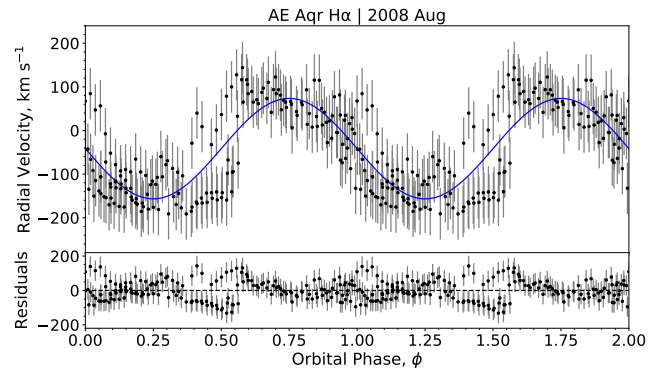


Figure 2. Radial velocity curve of $H\alpha$ for the 2008 Aug observation run.

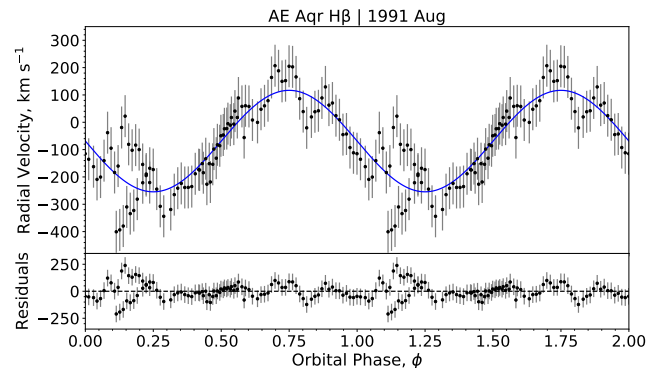


Figure 3. Radial velocity curve of $H\beta$ for the 1991 Aug observation run.

3.1 Orbital parameters

To measure the radial velocity of the emission line wings, we have used the CONVRV task within the RVS AO package in IRAF¹ written by J. Thorstensen (2008, private communica-

¹ IRAF is distributed by the National Optical Astronomy Observatories, which are operated by the Association of Universities for

tion), which convolves the line profile with an antisymmetric function and interprets the root of the convolution as the midpoint of the line profile, as per the algorithm described by Schneider & Young (1980). In particular we implemented the standard double-Gaussian (GAU2) option as our convolution function (Shafter et al. 1986), which traces the radial velocity of the profile wings. This method requires us to specify two parameters: a Gaussian width and the separation between the centres of the antisymmetric pair of Gaussians.

Ideally a diagnostic diagram is performed to probe for the optimal values of the parameters of the convolution function (Shafter 1983; Shafter et al. 1986). However, given that the H α and H β emission lines of AE Aqr exhibit a very unstable behaviour, we were unable to perform an enough number of stable convolutions to make a diagnostic diagram. Therefore we had to visually inspect the convolutions that yielded a solution, and chose the parameters that produced the most stable sinusoidal pattern. These parameters are listed in Table 1, while the radial velocity curves produced with these parameters are depicted in Figures 1, 2, and 3. Note that in some phase intervals the radial velocities show considerable fluctuations and therefore the sinusoidal fit is not a simple one.

We are aware that this is not the optimal approach to find the best K_1 , γ , and HJD_0 values, but it will serve the purpose of detecting a sinusoidal modulation that will aid us in making a good approximation for the semi-amplitude K_1 by fitting the data to a circular orbit (see Equation 1).

3.1.1 H α emission line

For the observations of Aug 2000, we used a Gaussian width of 35 pixels and a separation of 122 pixels. The radial velocity curve of this run is displayed in Figure 1. The orbital fit (blue curve) yielded a semi-amplitude value of $K_1 = 114 \pm 8 \text{ km s}^{-1}$.

The Aug 2008 radial velocities, shown in Figure 2, were produced with a Gaussian width of 14 pixels and a separation of 121 pixels, yielding $K_1 = 115 \pm 6 \text{ km s}^{-1}$, which is consistent with the value of Aug 2000. However, this run shows more variability, being especially erratic throughout the phase interval $\sim 0.25 - 0.50$. The orbital parameters of H α are shown in Table 2.

Because the radial velocity data of Aug 2000 is the most stable of the three runs analysed, we adopt $K_1 = 114 \pm 8 \text{ km s}^{-1}$ as our best approximation to the orbital motion of the white dwarf. This value is consistent within 2σ to that obtained in Paper I, wherein the rotational velocity of the secondary star was measured to indirectly derive $K_1 = 101 \pm 3 \text{ km s}^{-1}$. The same consistency holds with the value derived from the pulse timing data by Eracleous et al. (1994), of $K_1 = 102 \pm 2 \text{ km s}^{-1}$.

Taking our direct measurement of the value $K_1 = 114 \pm 8 \text{ km s}^{-1}$; the semi-amplitude of the secondary $K_2 = 168 \pm 1 \text{ km s}^{-1}$, obtained in Paper I; and using the fixed value of the orbital period of $P = 0.4116554800(2)$, we calculate:

Table 1. Parameters of the used convolution functions (Double Gaussian). See text.

Conv. Func. Parameter	Aug 2000 H α	Aug 2008 H α	Aug 1991 H β
Width (Pixels)	35	14	250
Separation (Pixels)	122	121	507

Table 2. Orbital Parameters obtained from the H α line.

Orbital Parameter	Aug 2000 H α	Aug 2008 H α
γ (km s^{-1})	-73 ± 5	-41 ± 4
K_1 (km s^{-1})	114 ± 8	115 ± 6
HJD_0 (2439030+)	0.865 ± 0.004	0.967 ± 0.003
P_{orb}^* (days)	$0.4116554800(2)$	$0.4116554800(2)$

*Fixed

$$M_1 \sin^3 i = \frac{PK_2(K_1 + K_2)^2}{2\pi G} = 0.58 \pm 0.03 M_\odot \quad (2)$$

and,

$$M_2 \sin^3 i = \frac{PK_1(K_1 + K_2)^2}{2\pi G} = 0.39 \pm 0.05 M_\odot \quad (3)$$

Assuming an inclination of $i = 70^\circ \pm 3$ yields a value of the mass of the white dwarf of $M_1 = 0.69 \pm 0.06 M_\odot$; while for the secondary it results in a mass of $M_2 = 0.47 \pm 0.07 M_\odot$. These values are consistent within the errors with those obtained in Paper I. However, the indirect derivation of K_1 is still more reliable than our direct measurement. Therefore, we will adopt the values of the mass parameters published in Paper I, of $M_1 = 0.63 \pm 0.05 M_\odot$ and $M_2 = 0.37 \pm 0.04 M_\odot$, to produce the Doppler tomograms in Section 4.

3.1.2 H β emission line

Variations in the line profile of H β for the 1991 observations rendered a double-Gaussian whose parameters were difficult to find. A Gaussian width of 250 pixels and a separation of 507 pixels were used. This run presents considerable fluctuations in the phase intervals of $\sim 0.00 - 0.25$ and $\sim 0.60 - 0.85$, as shown in Figure 3, where the semi-amplitude yielded a high value of $K_1 = 185 \pm 11 \text{ km s}^{-1}$. The orbital parameters of this run are exhibited in Table 3. The semi-amplitude value of H β is inconsistent from those obtained above for H α ; we address a possible cause for this deviation in Section 4.2.

4 DOPPLER TOMOGRAPHY

Doppler Tomography is a spectroscopy technique that uses the phase resolved emission line profiles to map the accretion

Table 3. Orbital Parameters obtained from the $H\beta$ line.

Orbital Parameter	Aug 1991 $H\beta$
γ (km s^{-1})	-68 ± 7
K_1 (km s^{-1})	185 ± 11
HJD_0 (2439030+)	0.840 ± 0.003
P_{orb}^* (days)	$0.4116554800(2)$

*Fixed

flow in velocity space. A detailed formulation of this technique can be found in [Marsh & Horne \(1988\)](#).

In Section 4.1, we describe the Tomography of the $H\alpha$ lines from Aug 2000 and Aug 2008, and show the resulting images in Figure 4. To produce said tomograms, we used a newly developed PYDOPPLER² python code. This code uses the original FORTRAN programs, developed by [Spruit \(1998\)](#) for an IDL environment. As explained in Section 3.1.1, we adopted the mass parameters of $M_1 = 0.63 \pm 0.05 M_\odot$ and $M_2 = 0.37 \pm 0.04 M_\odot$, calculated in Paper I, to produce the Tomography images.

We were not able to construct the $H\beta$ tomogram from the observing run of Aug 1991, as the variations of this emission line throughout the orbital period did not allow the convergence of a reliable image. Instead we present the phase resolved profile of the emission line in Figure 5. This variations are described in detail in Section 4.2.

4.1 $H\alpha$ Tomography

The Doppler Tomography of Aug 2000 is exhibited in the top right panel of Figure 4. Its respective observed and reconstructed spectrograms are shown in the top left panels. With the same layout, in the bottom panels, we present the Aug 2008 results.

The trailed spectra of Aug 2000 shows a broad single-peaked structure all throughout the orbit. The structure becomes especially broad in the orbital phase interval of ~ 0.00 – 0.05 . There is a decrease of the relative flux of the profile in the interval ~ 0.55 – 0.75 . The line profile presents a clear sinusoidal modulation, as expected from the radial velocity analysis (See Section 3). Its tomography shows a blob-like emission in the lower quadrants centred close to the velocity coordinates of the white dwarf, with its intensity decreasing radially and lacking azimuthal symmetry.

The trailed spectra of Aug 2008 also exhibits a single-peaked structure, with a decrease of relative flux in the intervals spanning ~ 0.00 – 0.10 and ~ 0.40 – 0.55 . The sinusoidal modulation in this run is also evident. The Doppler Tomography again shows an asymmetric blob, with maximum intensity in the lower left quadrant centred at $\sim (-50, -10)$, from where the flux decreases radially outward.

The overall structure of both tomograms is very similar to those obtained by [Welsh et al. \(1998\)](#). These authors interpret such structure, concentrated in the lower quadrants, as

a consequence of the propeller action caused by the rapidly-rotating magnetic white dwarf.

4.2 $H\beta$ Line Profile

The highly-variable and disrupted nature of the $H\beta$ emission line profile along the orbital phase, exhibited in the observed trailed spectrum in Figure 5, did not allow us to produce a dependable tomography. The spectrogram shows a broad single-peaked profile that shifts towards negative velocities in the orbital phase interval of ~ 0.00 – 0.20 . The profile suddenly narrows at phase ~ 0.25 ; but it then considerably broadens in the interval ~ 0.30 – 0.50 , while drifting towards positive velocities. Within the phases ~ 0.50 – 0.90 , the single-peaked profile again narrows down, and the midpoint of the emission is abruptly displaced to positive velocities. In this same narrow stage the profile briefly oscillates, initially moving in a negative direction, reaching a minimum velocity at phase ~ 0.75 , and again drifting towards the positive direction until phase ~ 0.90 . At this stage the trail becomes disrupted with the profile *leaping* back to the left and recovering a broader structure, which is preserved until the end of the orbit.

This complex and asymmetric behaviour exhibited in the spectrogram not only impeded the construction of a tomogram, but also made difficult to produce a radial velocity curve, which could explain the highly discrepant semi-amplitude value of $K_1 = 185 \pm 11 \text{ km s}^{-1}$, obtained for this emission line in Section 3.1.2.

5 DISCUSSION

We made a complementary study to that performed in Paper I, using the original spectroscopic data, by analysing the $H\alpha$ and $H\beta$ Balmer emission lines. As demonstrated by [Welsh et al. \(1998\)](#), tracking the orbital motion of the white dwarf using the emission lines is a very unreliable method for AE Aqr. However the propeller model (see [Wynn et al. 1997](#), and references therein) does predict a small fraction of accretion of the material onto the white dwarf, meaning that not all of it is ejected by the propeller action. Also, the narrow component of the Balmer emission lines observed by [Reinsch & Beuermann \(1994\)](#) is in anti-phase to the absorption lines of the red dwarf, which suggests its origin is near the primary star. Furthermore, the presence of an accretion disc with a variable nature cannot be discarded, as suggested by the axisymmetric magnetohydrodynamics simulations put forward by [Blinova et al. \(2019\)](#).

With this in mind, in Section 3, we performed several radial velocity analyses of the emission lines, from which our main result was to find a reasonable value of $K_1 = 114 \pm 8 \text{ km s}^{-1}$ for $H\alpha$, during the observing run of Aug 2000. This value is consistent within 2σ with the indirect measurements obtained in Paper I and [Eracleous et al. \(1994\)](#), whose analyses yielded $K_1 = 101 \pm 3 \text{ km s}^{-1}$ and $K_1 = 102 \pm 2 \text{ km s}^{-1}$, respectively. This consistency implies that, at least for Aug 2000, we were able to track the orbit of the white dwarf by tracing the wings of the emission line profile (which presumably arise from high velocity material orbiting close to the primary star). This can be interpreted as possible observational evidence of material orbiting the white dwarf. This claim is further supported by the fact that, during the observations of Aug 2000, the

² Available at <https://github.com/Alymantara/pydoppler>

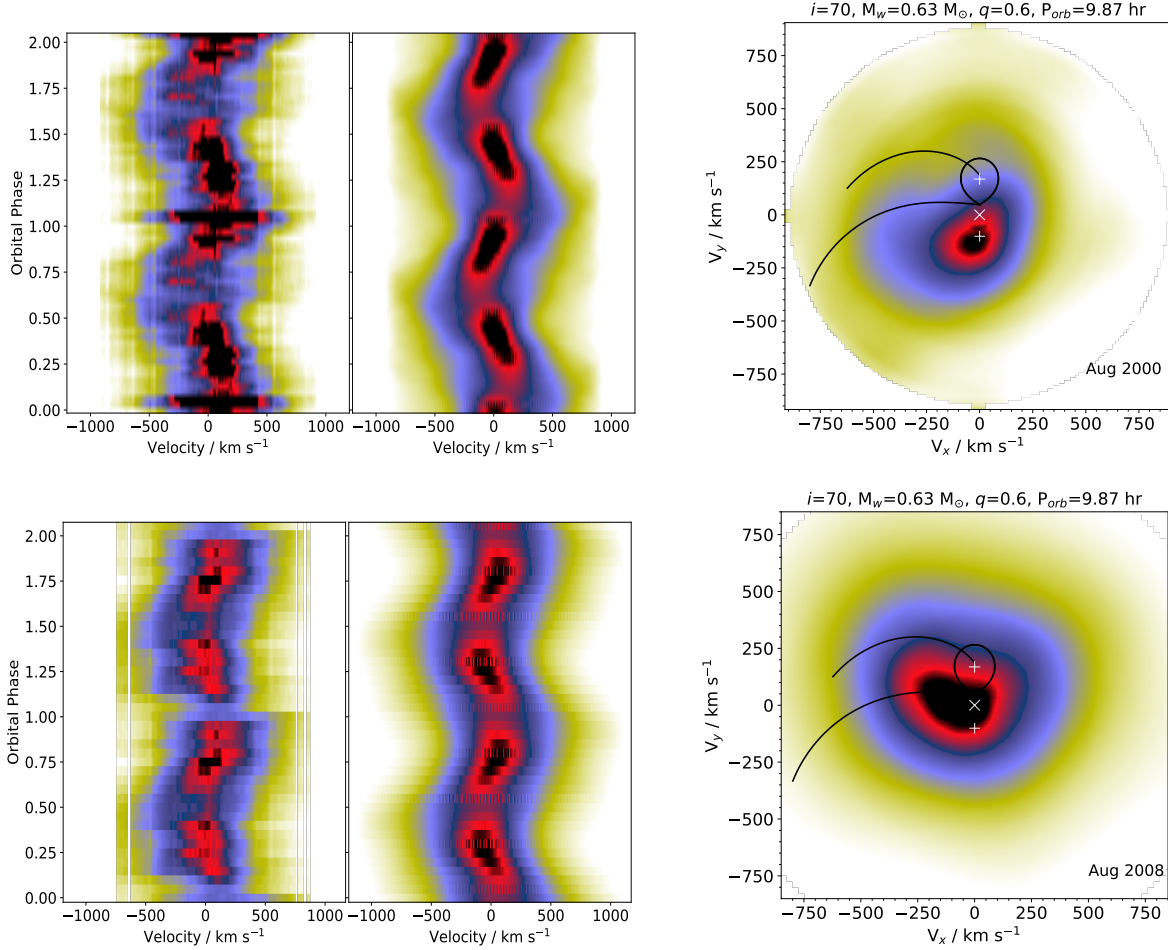


Figure 4. *Top:* Trailed spectrum of the $H\alpha$ emission line for the observed data of 2000 Aug (*left*), the reconstructed trailed spectrum (*middle*), and the Doppler Tomography (*right*). *Bottom:* Trailed spectrum of the $H\alpha$ emission line for the observed data of 2008 Aug (*left*), the reconstructed trailed spectrum (*middle*), and the Doppler Tomography (*right*). The relative flux is depicted in a scale of colours, where black represents the highest intensity, followed by red, then blue, and finally yellow. Various features in the tomographies are marked as follows: the white crosses are the velocities (from top to bottom) of the secondary star, the centre of mass and the primary star. The Roche lobe of the secondary is shown around its cross. The Keplerian and ballistic trajectories of the gas stream are marked as the upper and lower curves, respectively. See text for further discussion.

Doppler Tomography shows the emission centred around the position of the primary star. Moreover, the observations of Aug 2008 yielded a value of $K_1 = 115 \pm 6 \text{ km s}^{-1}$, in good agreement with the 2000 run.

Even if we did detect material orbiting the primary star, our spectrograms and Tomograms do not show the characteristic signatures of a fully formed accretion disc (Marsh & Horne 1988). In fact, the overall shape of our tomograms was consistent with that exhibited in Welsh et al. (1998), where the concentration of emission in the lower left quadrant and the azimuthal asymmetry is conjectured to be caused by the propeller mechanism (e.g. Wynn et al. 1997; Ikhsanov et al. 2004). Although, as mentioned above, in Aug 2000 we find the centre of emission near the position of the white dwarf; a feature not observed previously nor expected in the propeller model.

For the observing run of Aug 1991, we made a radial velocity analysis of $H\beta$, obtaining $K_1 = 185 \pm 11 \text{ m s}^{-1}$. This value disagrees with the $H\alpha$ results. However, we attribute this dis-

crepancy to the highly variable behaviour of $H\beta$ exhibited in its trailed spectrum (see Section 4.2).

6 CONCLUSIONS

Using the spectroscopic data gathered for several epochs in Paper I, we have studied the emission lines of AE Aqr and found observational evidence of material orbiting the rapidly rotating white dwarf. Specifically, the radial velocity analysis of the most stable of our observing runs (Aug 2000), yields a semi-amplitude value consistent with previously published results obtained via indirect methods. Also, the Doppler Tomography obtained from this run, shows that the emission is centred around the position of the white dwarf. This is not characteristic of the predictions made in the propeller model.

It is made evident in our analysis of the $H\beta$ emission line, that considerable limitations are posed when tracking the velocity of the emission lines. However, due to the feasibility that these lines are indeed originated in the re-

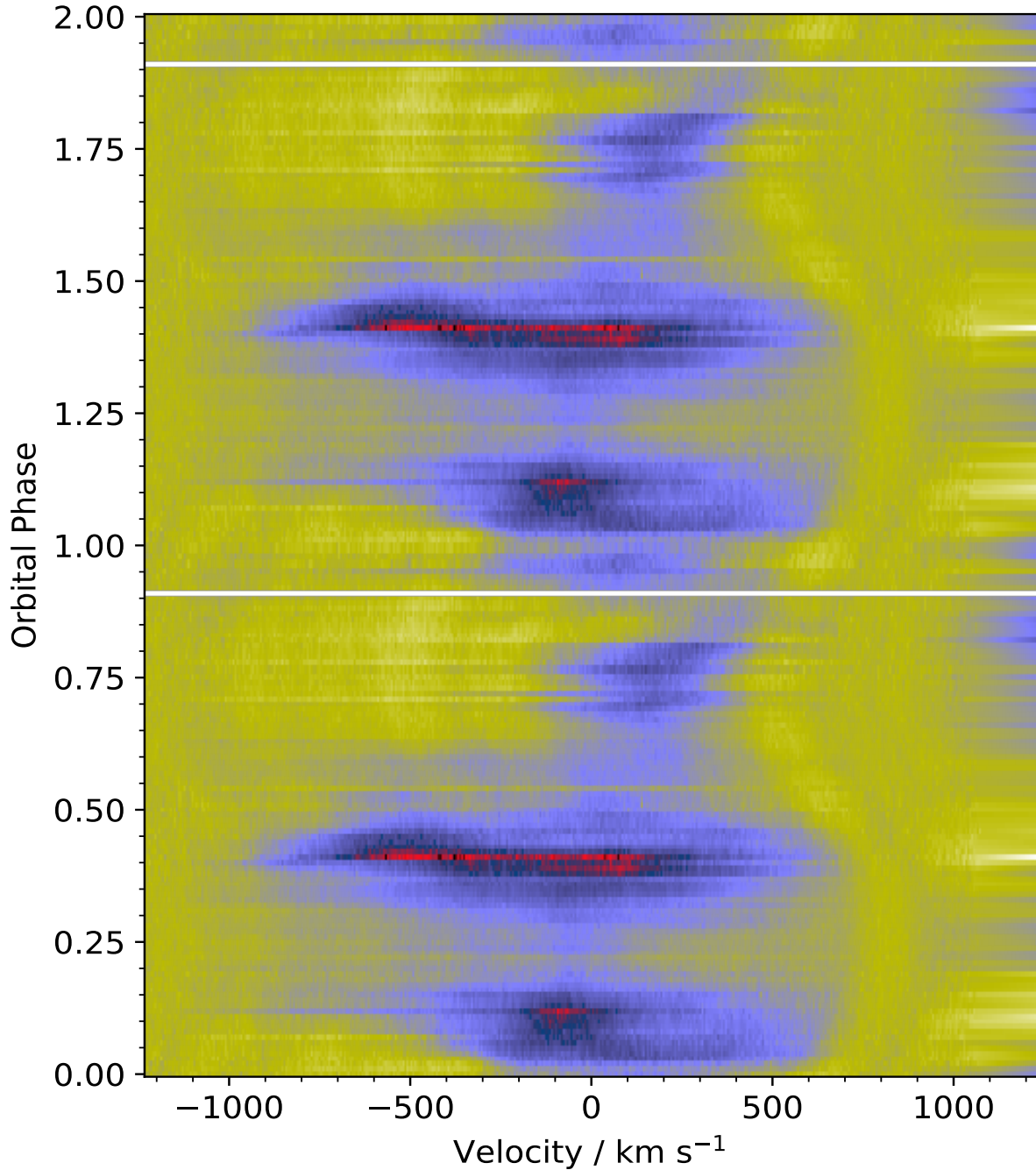


Figure 5. Phase resolved line profiles of $H\beta$. The relative flux is depicted in a scale of colours, where black represents the highest intensity, followed by red, then blue, and finally yellow. For illustrative purposes the orbit is reproduced a second time.

gions around the primary component, we consider our best estimate of the semi-amplitude value obtained for $H\alpha$, of $K_1 = 114 \pm 8 \text{ km s}^{-1}$, as a good approximation of the orbital motion of the white dwarf.

ACKNOWLEDGEMENTS

The authors are indebted to DGAPA (Universidad Nacional Autónoma de México) support, PAPIIT projects IN114917 and IN103120. This research made use of ASTROPY, a

community-developed core PYTHON package for Astronomy (Astropy Collaboration et al. 2013), Python’s SciPy signal processing library (Virtanen et al. 2020) and MATPLOTLIB (Hunter, J. D. 2007). We would also like to thank the anonymous referee, whose comments helped improve the content of this article.

DATA AVAILABILITY

The data underlying this article can be shared on request to the corresponding author.

REFERENCES

- Astropy Collaboration et al., 2013, *A&A*, 558, A33
- Blinova A. A., Romanova M. M., Ustyugova G. V., Koldoba A. V., Lovelace R. V. E., 2019, *Monthly Notices of the Royal Astronomical Society*, 487, 1754
- Cropper M., 1986, *MNRAS*, 222, 225
- Cropper M., 1990, *Space Sci. Rev.*, 54, 195
- Echevarría J., Smith R. C., Costero R., Zharikov S., Michel R., 2008, *Monthly Notices of the Royal Astronomical Society*, 387, 1563
- Eracleous M., Horne K., Robinson E. L., Zhang E.-H., Marsh T. R., Wood J. H., 1994, *ApJ*, 433, 313
- Horne K., Marsh T. R., 1986, *Monthly Notices of the Royal Astronomical Society*, 218, 761
- Horne K., Wade R. A., Szkody P., 1986, *MNRAS*, 219, 791
- Hunter, J. D. 2007, *Computing In Science & Engineering*, 9, 90
- Ikhsanov N. R., Neustroev V. V., Beskrovnaya N. G., 2004, *A&A*, 421, 1131
- Isakova P. B., Ikhsanov N. R., Zhilkin A. G., Bisikalo D. V., Beskrovnaya N. G., 2016, *Astronomy Reports*, 60, 498
- Kafka S., Honeycutt R. K., Howell S. B., Harrison T. E., 2005, *AJ*, 130, 2852
- Marsh T. R., Horne K., 1988, *MNRAS*, 235, 269
- Patterson J., 1979, *ApJ*, 234, 978
- Patterson J., 1994, *PASP*, 106, 209
- Reinsch K., Beuermann K., 1994, *A&A*, 282, 493
- Robinson E. L., Shafter A. W., Balachandran S., 1991, *ApJ*, 374, 298
- Schneider D. P., Young P., 1980, *ApJ*, 238, 946
- Shafter A. W., 1983, *ApJ*, 267, 222
- Shafter A. W., Szkody P., Thorstensen J. R., 1986, *ApJ*, 308, 765
- Smak J., 1971, *Acta Astron.*, 152, 219
- Spruit H. C., 1998, arXiv e-prints, [pp astro-ph/9806141](https://arxiv.org/abs/pp astro-ph/9806141)
- Virtanen P., et al., 2020, *Nature Methods*, 17, 261
- Walker M. F., 1965, *Sky & Tel.*, 29, 23
- Warner B., 1995, *Cambridge Astrophysics Series*, 28
- Warner B., Nather R. E., 1971, *MNRAS*, 152, 219
- Welsh W. F., Horne K., Gomer R., 1998, *MNRAS*, 298, 285
- Wynn G. A., King A. R., Horne K., 1997, *MNRAS*, 286, 436

This paper has been typeset from a $\text{\TeX}/\text{\LaTeX}$ file prepared by the author.